Progress In Electromagnetics Research C, Vol. 137, 123–138, 2023

A Compact Dual-Band CPW-Fed Slotted-Ring Monopole Antenna with Circular Fractal Elements for WiMAX and C Bands Applications

Dhirgham K. Naji*

Abstract—This paper presents a new compact dual-band slotted-ring monopole antenna (SRMA) with circular fractal elements (CFEs) design for WiMAX and C bands applications. Good improvements are obtained in widening the upper-frequency band of the proposed antenna and in miniaturizing its overall size. Antenna miniaturization is accomplished by employing a coplanar waveguide (CPW)-fed fractal-shaped SRMA loaded at its inside and outside of the ring's peripherals by two types of CFEs, namely, CFE1 and CFE2. The dual-band capability of antenna is realized by introducing in its ring's center a circular slit to act as a key parameter for band rejection characteristic. The design procedure starts from a conventional circular monopole antenna (CMA), and evolution steps of antenna are performed until achieving the proposed CPW-fed SRMA with aforementioned features. The simulated results in terms of reflection coefficient, gain, efficiency, and radiation patterns are obtained by using CST MWS and HFSS programs. Due to the agreement between the CST and HFSS simulated results, the prototype of the antenna is fabricated on one side of an FR4 substrate with a volume of $20 \times 22 \times 0.8\,\text{mm}^3$. Then the measured reflection coefficient is conducted, and it agrees well with the simulated counterpart. As observed from measurement, the antenna operates at two distinct bands of 3.15–3.75 GHz and 5.02–7.58 GHz that exhibits the proposed antenna to cover WiMAX, WLAN, C-, 4G LTE, 5G, and Sub-6 GHz bands. Also, the proposed antenna exhibits an acceptable gain and efficiency across the operating bands along with omnidirectional radiation pattern.

1. INTRODUCTION

Due to the continuous development of portable wireless communication devices such as laptops, tablets, and smartphones, it is urgent to make these systems to be miniaturized in size and operate in more than one communication band. Nevertheless, designing a miniature multiband antenna satisfying the desired performance is considered one of the most difficult tasks and requires a lot of tedious work. However, such miniature, multiband antennas are needed by most portable wireless devices. Consequently, monopole antennas (MAs) are considered the key choice for satisfying both the aforementioned requirements in wireless communication systems; size miniaturization and characteristic of multiband operation. This suitability of miniaturizing the MAs for operating in the multiband communication standards is due to their attractive features including light weight, low cost, and ease of integration with other microwave integrated circuits [1]. Mainly, two types of feeding methods are used for realizing this type of antenna, microstrip line and coplanar waveguide (CPW)-fed based structures. The CPW-fed technique has many advantages with respect to the microstrip feeding structure like single layer metallization, low dispersion, the ability for controlling the characteristic impedance, low radiation loss,

Received 24 July 2023, Accepted 17 August 2023, Scheduled 2 September 2023
* Corresponding author: Dhirgham Kamal Naji (dhrgham.kamal@gmail.com).
The author is with the Department of Electronic and Communications Engineering, College of Engineering, Al-Nahrain University, Baghdad, Iraq.

and simplicity in structure by avoiding the use of via holes and shorting pins [2, 3]. Thus, due to the foregoing features, the CPW-fed mechanism is adopted in this work for feeding the proposed antenna.

There exist numerous methodologies to design reduced-size antennas that have wide bandwidth or can cover multibands. However, antenna miniaturization is a compromise between multiband operation characteristics and maximization of gain and efficiency [4]. Some of these methods use slot or strip elements in the patch or ground plane, incorporating shorting pins or via holes, and defected ground structure [5–8]. For instance, Ref. [5] presents a compact tri-band MA composed of an inverted-L slot element embedded in a π-shaped slot element. It operates at three bands for $|S_{11}| < -10$ dB: Band 1 (2.37–2.52 GHz), Band 2 (3.35–3.9 GHz), and Band 3 (4.97–7.85 GHz). In [6], a compact tri-band triangular MA has been designed by using various lengths of inverted L-shaped stubs for multiband operation, and via shorting pin was connected from the back side of the substrate to the longest stub for miniaturization. It has a compact size of $20 \times 15 \times 1.6\,\text{mm}^3$, and yet it has a complex structure for adopting shorting pin in the design. A compact triple-band antenna was present in [7] that utilized a microstrip-fed line as a patch formed by etching on it an inverted L-shaped slot, and a defected ground structure was printed in the other side of the substrate. It covers the 2.39–2.51 GHz, 3.15–3.91 GHz, and 4.91–6.08 GHz frequency bands. A circular monopole antenna with packed four T-shaped strips was proposed in [8] to cover wideband frequencies ranging from 3.09 to 4.15 GHz. However, the works in [7] and [8] have simple structures and satisfy the desired performance, but their sizes are large.

Recently, many CPW-fed MAs have been designed for wideband/dual-band operation suitably covering the 3.5 GHz (3.3–3.8 GHz) WiMAX band or/and 5.2-/5.8-GHz WLAN band and (4–8 GHz) C band. These include fractal, meander, and metamaterial (MTM) construction. For instance, Ref. [9] presents a fractal-based hexagon-shaped ring patch antenna with CPW feeding to generate two resonance modes, 3.5-GHz WiMAX and 5.5-GHz WLAN. It provides dual bands with an overall size of FR4 substrate of $22 \times 22 \times 1.6\,\text{mm}^3$ and exhibits omnidirectional radiation with 2.04 and 3.44 dBi of peak realized gains over the lower and upper bands, respectively. A 9-point star-shaped fractal monopole antenna with a band-notched characteristic in [10] is realized by inserting in its ground planes one pair of L-shaped slots to satisfy the two bands, (3.05–3.84 GHz) and (5.15–5.825 GHz) applications. As another example, a new rectangular grounded CPW feed line consists of two arms in the radiating patch and two strip elements on both sides of the feed line, and a partial ground plane on the back side of the substrate is presented in [11]. A dual-band operation is yielded from this designed antenna, (3.06–3.89 GHz) and (5.14–5.93 GHz) bands. In [12], a compact meandered fork-shaped MA is proposed for operating at (3.5/5.5 GHz) WiMAX, (5.2/5.8 GHz) WLAN, and C bands. This antenna is printed on an FR4 substrate of size $21 \times 21 \times 1.6\,\text{mm}^3$ and has a stable gain with higher radiation efficiency. A dual-band antenna is presented in [13], constructed from a vertical bow-tie-shaped radiating patch and two unsymmetrical ground planes. The antenna has dual working bands of 3.24–8.29 GHz and 9.12–11.25 GHz. In [14], a semi-circular MA with a CPW-fed structure, tapered-ground plane, and a folded U-shaped slot introduced in the patch is proposed. The antenna is characterized by a simple geometry of $17 \times 18 \times 0.8\,\text{mm}^3$ and has dual operating bands of (3.4–3.7 GHz) and (5.725–5.875 GHz). A new concept in [15] is introduced for enhancing the bandwidth of the metamaterial (MTM) inspired hexagon-shaped ring patch radiator inspired by a single-ring resonator as a metamaterial element. Due to MTM loading, more compact dimensions $17 \times 20 \times 1.6\,\text{mm}^3$ and wider bandwidth ranging from 3.06 to 5.89 GHz are obtained by the designed antenna. In [16], a circularly-slotted antenna for dual-band operation is presented. It mainly comprises a wide circular slot, a CPW feeding strip, and two pairs of unequally inverted L strips connected to the ground plane. In the previous review, despite successfully presenting dual operating antennas, they are either large in size, have complex structures, or have narrow upper band.

In this paper, a compact dual-band MA for WiMAX and C bands applications is presented. The proposed antenna consists of a CPW-fed structure, a circular ring patch (CRP) radiator, a circular slit, and two types of circular fractal elements (CFEs) slots inscribed within, inside, and outside the CRP. All the elements of antenna are printed on one side of an FR4 substrate of dimensions $20 \times 22 \times 0.8\,\text{mm}^3$, and no metallization is presented on the other side. The proposed antenna is analyzed and simulated by using CST MWS, and HFSS simulator tool is adopted to validate the CST simulated results. The fabricated prototype of the optimized antenna is measured, and good agreement is obtained with the simulated results. Overall, the proposed antenna has a simple structure, operates in the desired two

bands for WiMAX and C bands applications with omnidirectional radiation, and acceptable gain and efficiency over the operating bands.

The rest of this paper is outlined as follows. Section 2 describes the antenna configuration, design consideration, and parametric analysis. An explanation of experimental and simulated results, and discussion is developed in detail in Section 3. The final section gives the conclusion.

2. CONFIGURATION, DESIGN CONSIDERATION, AND PARAMETRIC ANALYSIS OF THE PROPOSED ANTENNA

This section presents the proposed antenna configuration with details of design consideration. Seven evolution steps that initiated by a CMA and ending by achieving the proposed compact dual-band fractal slotted-ring monopole antenna (SRMA) are outlined. Then, the key geometric antenna parameters are analyzed and discussed.

2.1. Antenna Configuration

The geometry of the proposed antenna for WiMAX and C bands applications is shown in Fig. 1(a) (front view), 1(b) (isometric view), and 1(c) (prototype). The antenna structure mainly consists of

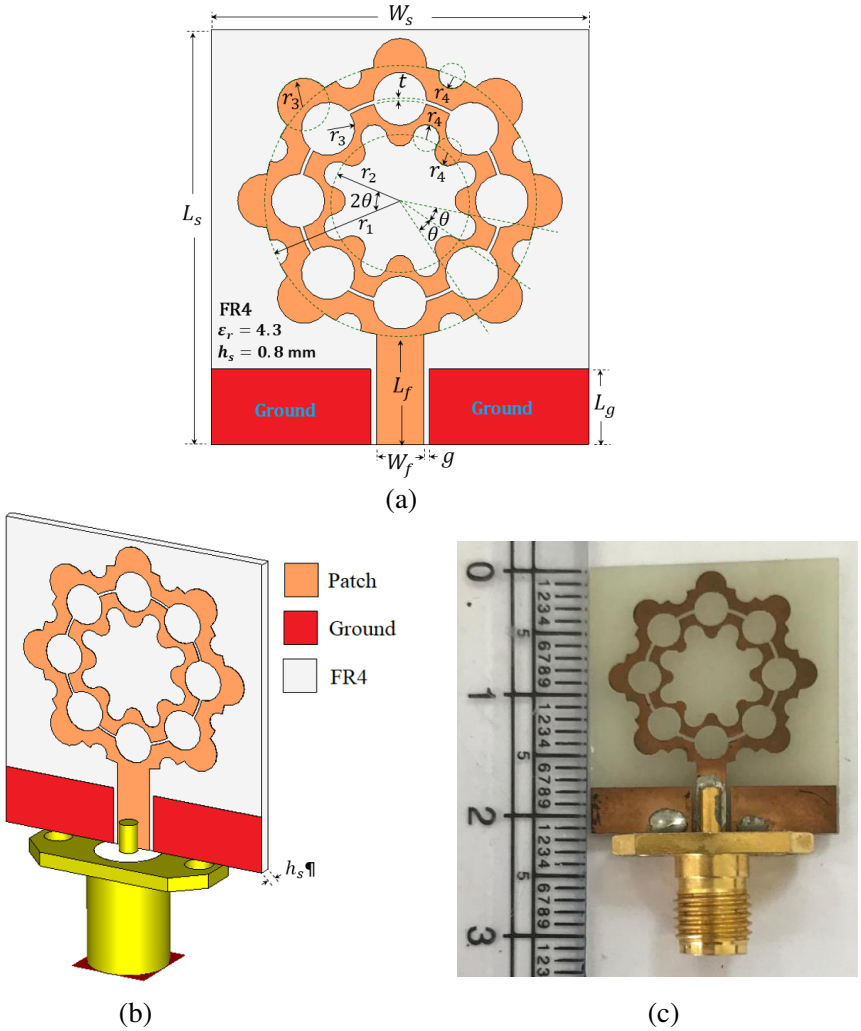

Figure 1. Configuration of the proposed fractal slotted-ring monopole antenna (SRMA): (a) Front view. (b) Isometric view. (c) Fabricated of the designed antenna.

a circular ring patch (CRP) radiator with outer and inner radii of r_1 and r_2, respectively, such that $r_1 = 2r_2$, and its lower side is connected to a 50-Ω CPW-fed stripline of length L_f and width W_f. A pair of symmetric rectangular ground planes of length L_g is laying at a gap distance (g) on both sides of the central strip. The patch, CPW stripline, and ground elements are printed on the same side of the FR4 substrate with overall dimensions $W_s \times L_s$ (20 mm × 22 mm), dielectric constant ($\varepsilon_r = 4.4$), height ($h_s = 0.8$ mm), while there is no metallization copper on the other side of the substrate. In order to have dual-band frequency spectrum with miniaturized size, two types of circle fractal elements (CFEs), namely CFE1 and CFE2 with radii r_3 and r_4, respectively, such that $r_3 = 2r_4$, are inscribed and added within, outside, and inside the CRP structure. As shown in Fig. 1(a), twenty-four of type CFE2 are inserted and added within, outside, and inside the CRP antenna radiator while fourteen of type CFE1 are inscribed and added within and outside the main CRP structure. To properly covering the WiMAX and C bands by the proposed antenna, the band-stop characteristic is realized by adding a circular slit with a thickness 't' within the CRP's center. A sub-miniature adapter (SMA) is connected to the CPW-fed stripline to be taken into consideration in CST MWS and HFSS simulators for correctly modeling the designed antenna.

The detailed designs of CFE1 and CFE2 are shown in Figs. 2(a) and (b), respectively. As observed in Fig. 2(a), there are 4 small circles having radius r_3 (CFE1), and their centers are located at the circumference of the large circle (circle 1) of radius r_1. Each arc is drawn from the center of circle 1 with radius r_1, and angle θ covers one CFE1. Thus, r_3 can be related to r_1 by using the law of cosine as

$$r_3^2 = r_1^2 + r_1^2 - 2r_1 r_1 \cos(\theta/2) = 2r_1^2(1 - \cos(\theta/2)) \tag{1}$$

By assuming that $\theta = 22.5°$ (i.e., $\theta = 90°/4$) in (1), the approximation of r_3 can be rewritten as

$$r_3 = \sqrt{2}r_1\sqrt{1 - \cos(11.25°)} \cong 0.196r_1 \tag{2}$$

In the same manner, one can conclude from Fig. 2(b) that the radius r_4 of the CFE2 can be related to radius r_2 of circle 2 by

$$r_4 \cong 0.196r_2 \tag{3}$$

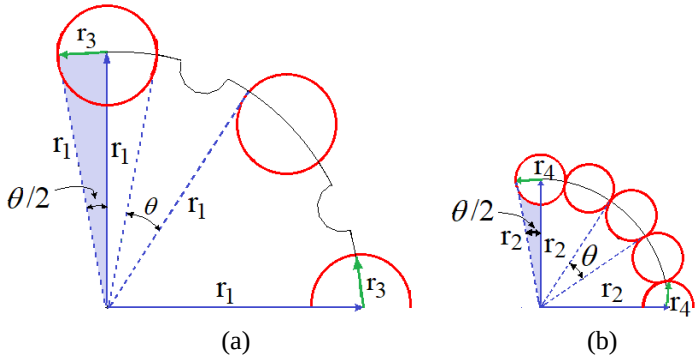

Figure 2. Detailed design of (a) CFE1 and (b) CFE2.

Table 1. Optimized parameters of the proposed antenna.

Parameter	Value (mm)	Parameter	Value (mm)
W_s	20	r_1	7.2
L_s	22	$r_2 = r_1/2$	3.6
W_g	8.45	r_3	1.410
L_g	4	$r_4 = r_3/2$	0.705
W_f	2.5	t	0.2
L_f	5.8	g	0.3

Since $r_1 = 2r_2$, then $r_3 = 2r_4$. Thus, if $r_1 = 7.2\,\text{mm}$, then $r_3 \cong 1.41\,\text{mm}$ and $r_4 \cong 0.705\,\text{mm}$, as observed in Table 1, which summarizes the optimized dimensions of the proposed antenna.

2.2. Design Evolution

This section presents in detail the design steps that must be followed to make the proposed antenna for operating within the desired frequency bands. Fig. 3 illustrates the seven evolution design steps as a development procedure ending by achieving the proposed antenna, named fractal SRMA, initiated from the reference antenna, named Ant 1 (or CMA). Fig. 4 illustrates the reflection coefficient plots for the seven different steps of evolved antenna, and their performance parameters are listed in Table 2.

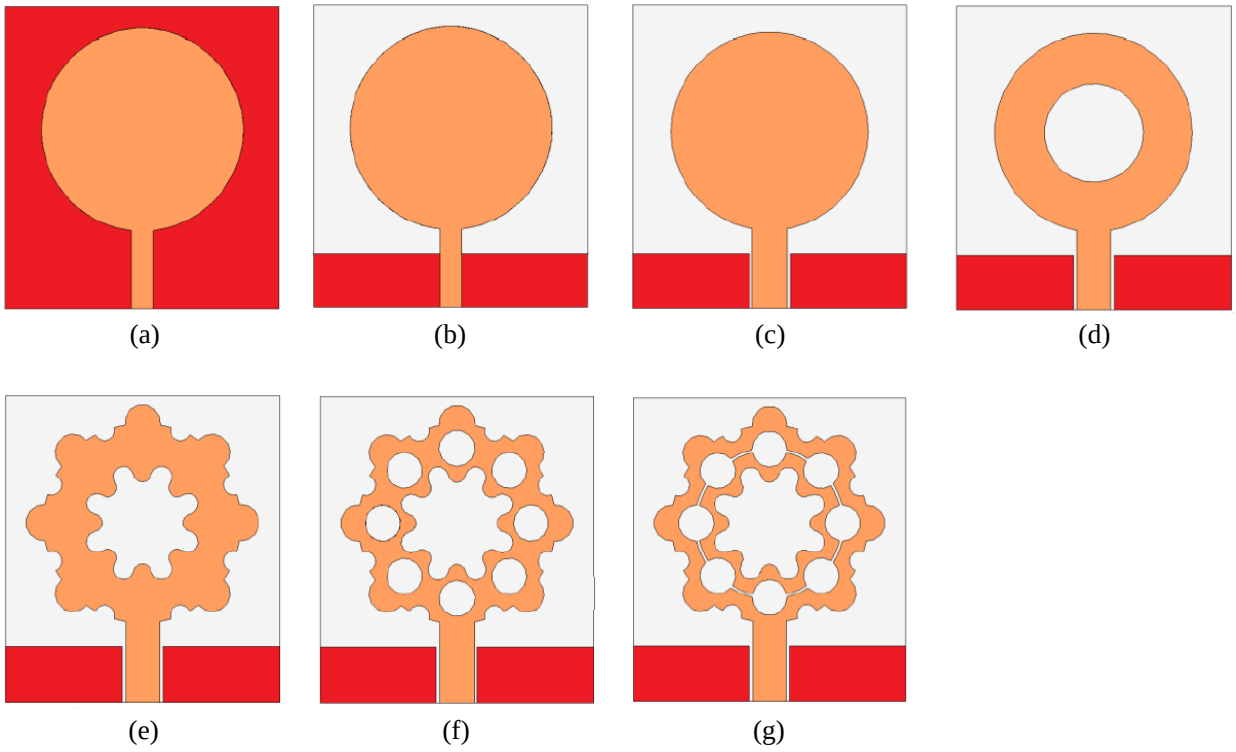

Figure 3. The evolution process of the proposed antenna. (a) Ant 1 (conventional circular monopole antenna (CMA)), (b) Ant 2 (CMA with partial ground), (c) Ant 3 (CPW-fed CMA), (d) Ant 4 (CPW-fed slotted-ring MA (SRMA)), (e) Ant 5 (fractal SRMA without inner CFE2), (f) Ant 6, (fractal SRMA without circular slit), (g) the proposed antenna (fractal SRMA).

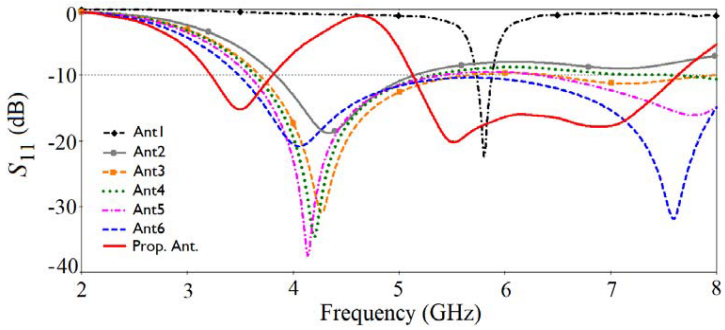

Figure 4. Simulated reflection coefficient characteristics of the seven different steps of evolved antenna.

Table 2. Performance parameters for the seven different steps of evolved antenna.

Design Evolution of the Proposed Antenna	Performance Parameters			
	−10 dB Impedance Bandwidth (GHz)	f_r (GHz)	$S_{11_{\|f_r}}$ (dB)	f_{notch} (GHz)
Ant 1	5.73–5.88	5.80	−22.36	NA
Ant 2	3.83–5.15	4.34	−18.84	NA
Ant 3	3.68–5.68 6.37>8.00	4.27 7.14	−31.00 −11.33	NA
Ant 4	3.64–5.33 7.48–>8.00	4.22	−34.65	NA
Ant 5	3.58–5.44 6.30–>8.00	4.13 7.78	−37.43 −16.13	NA
Ant 6	3.84–>8.00	4.06 7.60	−20.84 −31.87	NA
Proposed Ant.	3.22–3.80 5.07–7.64	3.5 5.5, 7.5	−15.27 −20.22, −17.75	4.55

Design Step 1:

In the first step, Ant 1 or the reference antenna, named as CMA, as shown in Fig. 4(a), is designed to operate at a specified resonance frequency (f_r), and both the substrate height (h_s) and dielectric constant (ε_r) are given. Then the radius r_1 of the circular patch is estimated by using the following design equations [17]

$$r_e = \frac{1.8142c}{2\pi f_r \sqrt{\varepsilon_r}} \tag{4}$$

$$r_1 = \frac{r_e}{\left(1 + \frac{2h_s}{\pi\varepsilon_r r_e}\left[\ln\left(\frac{\pi r_e}{2h_s}\right) + 1.7726\right]\right)^{1/2}} \tag{5}$$

where c is the speed of light in free space, and r_e is the effective radius of the patch due to the fringing field. Thus, substituting $f_r = 5.8\,\text{GHz}$ and $\varepsilon_r = 4.4$ in (4) gives $r_e = 7.2\,\text{mm}$. This value of r_e and $h_s = 0.8\,\text{mm}$ are used in (5) resulting in $r_1 = 7.0\,\text{mm}$. Then, Ant 1 is designed in a CST MWS by using $r_1 = 7.0\,\text{mm}$ as an initial value, then during simulation r_1 is optimized to be 7.35 mm. This antenna is printed on the front side of an FR4 substrate with a size $W_s \times L_s$ of (20 mm × 22 mm), and on its back side a full ground plane is used. The 50-Ω microstrip line is used for feeding antenna and has an optimized values for its width W_f and length L_f, 1.6 mm and 5.8 mm. As observed in Fig. 4 and Table 2, Ant 1 covers a narrow single frequency band specified by $f_r = 5.8\,\text{GHz}$ with $S_{11_{|f_r}} = -22.36\,\text{dB}$, and the impedance bandwidth (IBW) ($|S_{11}| < -10\,\text{dB}$) is 5.73–5.88 GHz.

Design Step 2:

To form Ant 2, a partial ground of length $L_g = 4\,\text{mm}$ is printed on the back side of the FR4 substrate instead of full ground, and all the other parameters of Ant 1 are kept unchanged. The reflection coefficient is as shown in Fig. 4 and Table 2, and Ant 2 can operate over IBW of 3.83–5.15 GHz and $f_r = 4.34\,\text{GHz}$. Thus, more bandwidth is achieved, but still, Ant 2 has only a single band.

Design Step 3:

At this step and the following phases of evolution in the design procedure, a CPW-feed is employed rather than a microstrip line for feeding the CMA by placing its circular patch of radius $r_1 = 7.2\,\text{mm}$

and a symmetric pair of ground structures of length $L_g = 4\,\text{mm}$ at the same side of FR4 substrate of dimensions $20\,\text{mm} \times 22\,\text{mm}$. The CPW central strip width $W_f = 2.5\,\text{mm}$, length $L_f = 5.8\,\text{mm}$, and gap ($g = 0.3\,\text{mm}$) are calculated via CST for assuring that a $50\,\Omega$ characteristic impedance is properly matched with the antenna's input impedance. Ant 3 as shown in Fig. 3(c) exhibits two separate working frequency bands of 3.68–5.68 GHz and 6.37–>8 GHz with single f_r produced in each band at around 4.27 and 7.14 GHz, as portrayed in Fig. 4. Thus, Ant 3 needs more developments to cover the required frequency bands.

Design Step 4:

A circular slot of radius $r_2 = 0.5r_1 = 3.6\,\text{mm}$ is inscribed within the CMA of Ant 3 to form Ant 4, as depicted in Fig. 3(d), having a CRP radiator. All the geometric parameters of Ant 3 remain unaltered when Ant 4 is constructed. As Fig. 4 and Table 2 show, this antenna can operate across dual-band of 3.64–5.33 GHz and 7.48–>8 GHz with $f_r = 4.22\,\text{GHz}$ generated at the lower band. Also, this antenna is required to be developed for operating over the desired bands.

Design Step 5:

In order to shift down the frequency band and resonance frequencies, a fractal technique is applied at the outside and inside of CRP for Ant 4. As observed in Fig. 3(e), two types of circle fractal elements, CFE1 and CFE2 with radius r_3 and r_4, respectively, are added and inscribed to Ant 4. As derived in Equations (1)–(3), $r_3 = 2r_4$, i.e., $r_3 \cong 1.41\,\text{mm}$ and $r_4 \cong 0.705\,\text{mm}$. As seen in Fig. 4, Ant 5 exhibits a working two bands of 3.58–5.44 GHz and 6.30–>8 GHz with one resonance mode in each band, 4.13 and 7.78 GHz. Again, Ant 5 is not able to cover the specified frequency bands, and more antenna evolution is required.

Design Step 6:

The addition of eight fractal elements from CFE1 at the center of the CRP of Ant 5 results in producing Ant 6, as depicted in Fig. 3(f). As Fig. 4 shows, Ant 6 is capable of operating in wide frequency band ranging from 3.84–>8 GHz. Two resonance frequencies are excited in this band of 4.06 and 7.06 GHz with corresponding $|S_{11}|$ of -20.48 and $-31.87\,\text{dB}$, respectively. Thus, the specified dual-band frequency range can be obtained by applying a band notched design method for Ant 6. This is achieved in the next step.

Design Step 7:

This is the final step in the design procedure that the proposed antenna is constructed. As shown in Fig. 3(g), a circular slit of thickness ($t = 0.2\,\text{mm}$) is added at the center of the CRP of Ant 6, and the proposed antenna, named fractal SRMA, is designed as a dual-band antenna. As shown in Fig. 4, the proposed antenna is efficiently operating at two separating bands of 3.22–3.80 GHz and 5.07–7.64 GHz. A stopband ranging from 3.80 to 5.07 GHz with a notch frequency f_{notch} of 4.55 GHz is created by employing the circular slit, which acts as a band notched design parameter. Thus, WiMAX (3.3–3.8 GHz), sub-6 GHz bands, LTE 42/43 (3.4–3.8 GHz), LTE 46 (5.15–5.925 GHz), WLAN (5.15–5.825 GHz), and C bands (4–8 GHz) are easily covered by the proposed antenna.

2.3. Parametric Analysis

As the miniaturized antenna is successfully designed to fulfil the desired frequency bands, a parametric analysis is carried out to investigate the effect of various geometric parameters on antenna reflection coefficient versus frequency performance and resonance frequencies f_{r1}, f_{r2}, and f_{r3} besides a notch frequency f_{notch}, which facilitates a more detailed antenna's operational principle. Six parameters, the radii r_1, r_2, r_3, and r_4 in addition to thickness t, and ground length L_g, are considered in this study. For each parameter under study, all the other parameters are kept at their optimum dimensions.

2.3.1. Varying Circular Ring Radii 'r_1' and 'r_2'

This step is used to inspect the influences of variations in r_1 and r_2 on reflection coefficient spectra and on notch and resonance frequencies. Figs. 5(a) and (b) show these results as r_1 and r_2 increase from 7.0 to 7.4 mm and from 3.6 to 4.0 mm, respectively. As noticed in Fig. 5(a), with the increment of r_1, all three resonances besides notch frequency shift downward. Still, the first resonance slightly decreases with increase in r_1 compared with the others. As Fig. 5(b) shows, when r_2 is varied from 3.6 to 4.0 mm, f_{r1} (f_{r2}) is less (more) influenced by this variation. Moreover, f_{r3} tends to increase while the other two resonances and f_{notch} decrease as r_2 is incremented. It is concluded from this study that r_2 has more effect on the resonances of the two bands than r_1 when they are allowed to be varied.

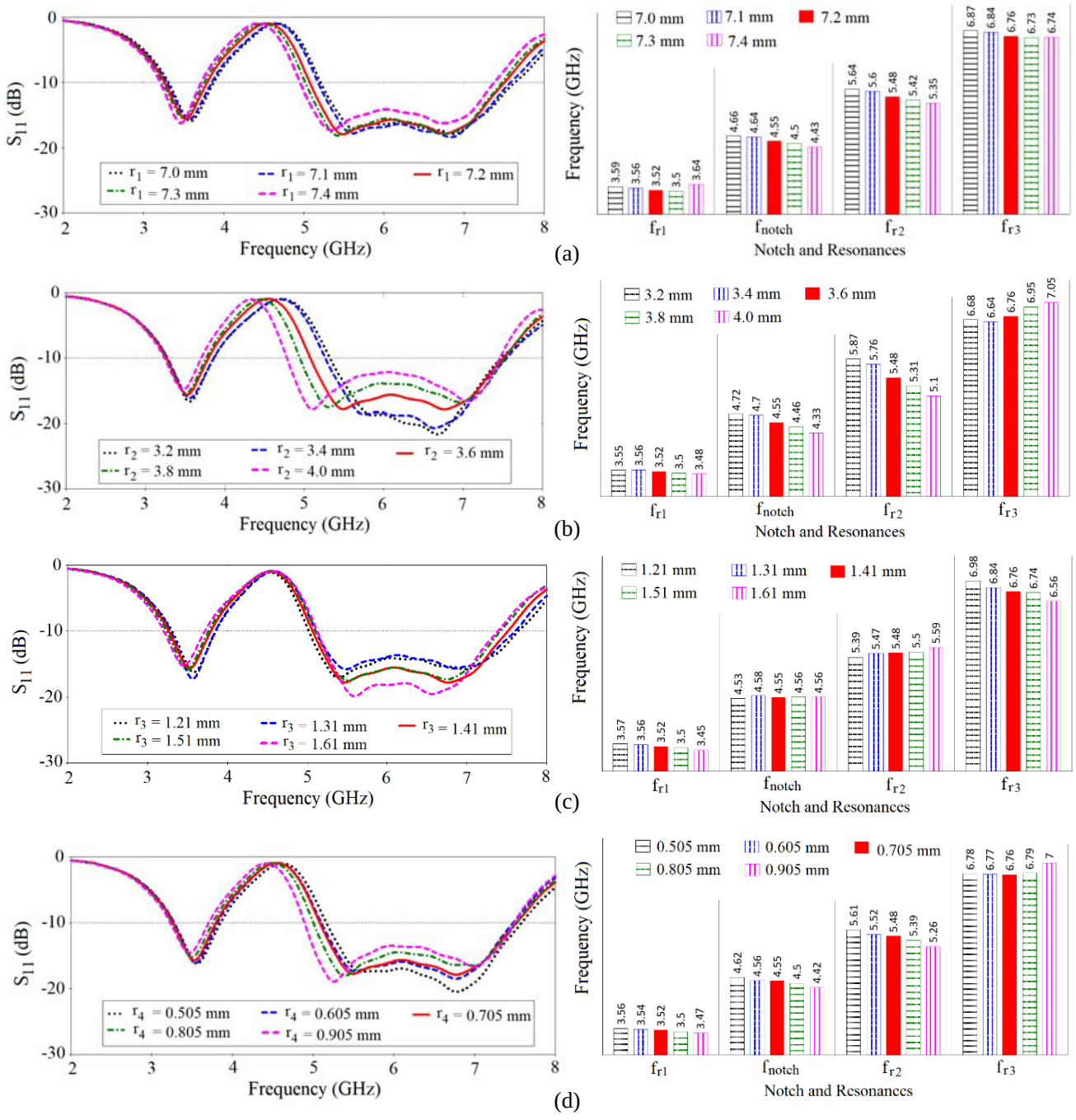

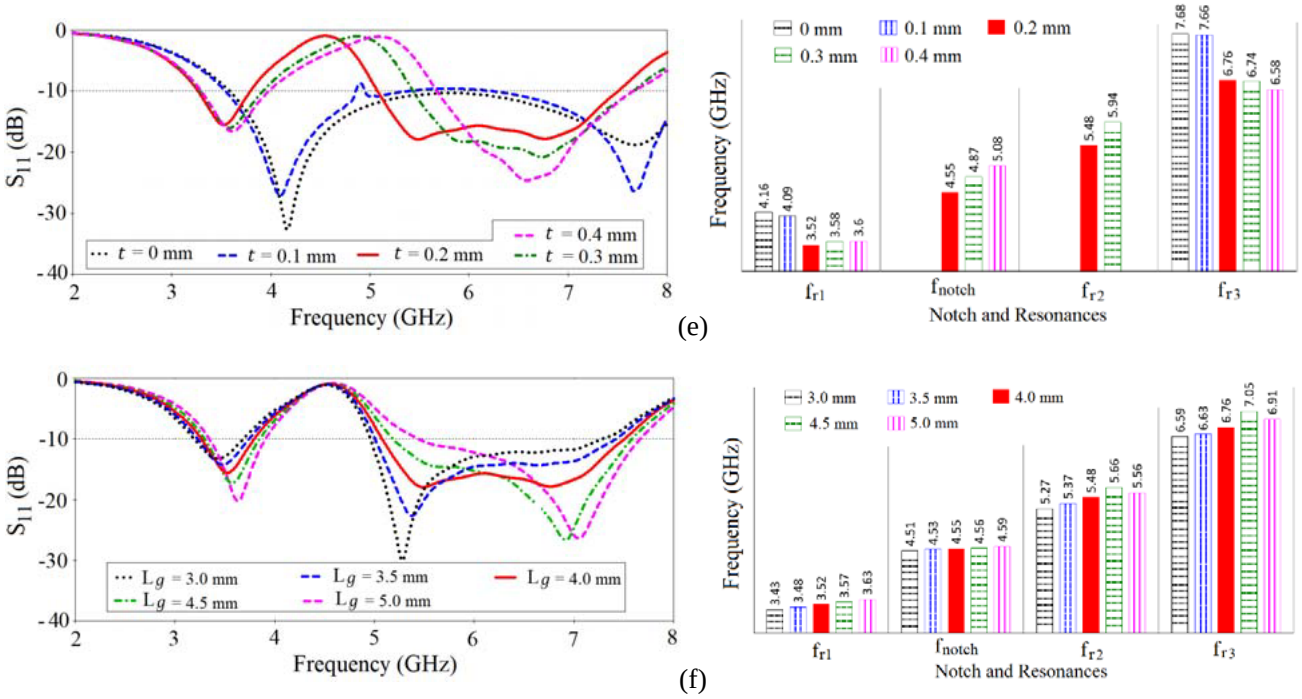

Figure 5. Impact of sweeping (a) outer radius r_1 and (b) inner radius r_2 of the circular ring, (c) radius r_3 of CFE1, (d) radius r_4 of CFE2, (e) thickness 't' of the circular slit, and (f) ground length L_g on the reflection coefficient alongside notch frequency and resonances of the proposed antenna.

2.3.2. Varying Circular Fractal Elements Radii 'r_3' and 'r_4'

Figures 5(c) and (d) depict the effects of changing the radii r_3 and r_4 of CFE1 and CFE2, respectively, on the reflection coefficient of the antenna and also on its resonance modes and notch frequency. As observed in Fig. 5(c), both f_{r1} and f_{r3} decrease; f_{r2} increases; and f_{notch} is nearly unaffected as r_3 is varied from 1.21 to 1.61 mm. On the other hand, increasing r_4 from 0.505 to 0.905 with a step size of 0.1 mm results in decreasing f_{r1}, f_{notch}, and f_{r2} whilst f_{r3} slightly increases, as shown in Fig. 5(d). Therefore, the parameter r_3 (r_4) is used to fine-tune the -10-dB higher (lower) frequency of the antenna's upper band.

2.3.3. Varying Thickness of the Circular Slit 't'

As previously discussed, the thickness of the circular slit t for the CRP of the proposed antenna is considered a key parameter for generating and fine-tuning the notched frequency band. Fig. 5(e) elucidates this claim by plotting the reflection coefficient characteristic alongside resonances and notch frequency as t is varied from 0 mm (without slit) to 0.4 mm. As Fig. 5(e) shows, no f_{notch} presents, and as a result, there is no notched frequency exhibited by the antenna when $t = 0$ mm. Also, the antenna has a single band ranging between 3.58 and greater than 8 GHz for $t = 0$ mm with two resonant mods, $f_{\text{r1}} = 4.16$ GHz and $f_{\text{r3}} = 7.68$ GHz, while f_{r2} is missed. As $t = 0.1$ mm, a narrow notched band ranging from 5.40 to 6.23 GHz and $f_{\text{notch}} \cong 5.8$ GHz with corresponding $|S_{11}|$ of only -9.63 dB is exhibited by the antenna. So, separating wide two frequency bands is achieved by antenna ranging from 3.54 to 5.40 GHz and from 6.23 to greater than 8 GHz with $f_{\text{r1}} = 4.09$ GHz, $f_{\text{r3}} = 7.66$ GHz, and f_{r2} is missed. As shown in Fig. 5(e), when t is increased from 0.2 to 0.4 mm, the notched band is largely increased and shifted to the higher frequency side. Also, the lower frequency of the lower band is nearly unaltered, and the higher frequency of the upper band is slightly increased as t is incremented from 0.2 to 0.4 mm. Moreover, only one resonance frequency f_{r3} with a peak reflection coefficient of the highest value is excited by the antenna, and f_{r2} gradually deteriorates and missed from the upper-frequency

band. Therefore, the optimum value of 0.2 mm given for t results in achieving the proposed antenna having the two operating bands, 3.22–3.80 GHz and 5.07–7.50 GHz. As stated earlier, the circular slit with dimension t can be considered the antenna's key geometric parameter by efficiently providing the desired notched frequency band suitable for the designed antenna to have the specified dual working bands.

2.3.4. Varying Ground Length 'L_g'

Figure 5(f) shows the effect of varying the ground length L_g on the proposed antenna. As noticed, the notch frequency f_{notch} is almost unchanged when L_g is varied from 3 to 5 mm. The first resonant frequency f_{r1} is increased as L_g increases, and the other two resonances f_{r2} and f_{r3} are increased for lower values less than 5 mm, and for $L_g = 5$ mm they are decreased. Moreover, the higher (lower) frequency of the second band is rapidly increased (decreased), and the higher frequency for the first band is more increased than decreased in its lower frequency as L_g is increased. Thus, the parameter L_g can be used efficiently for fine-tuning the separating upper and lower frequency bands and keeping the notched band between them unaltered.

3. EXPERIMENTAL AND SIMULATED RESULTS

In this section, experiment and simulation of antenna performance parameters, like reflection coefficient, surface current distribution, radiation efficiency, gain, and radiation patterns are presented and compared. First, the prototype of the designed antenna is fabricated, and then the measured and simulated reflection coefficients versus frequency characteristic are compared to validate the design principle. Two simulation programs, CST MWS and HFSS, are used for extracting the performance parameters. Finally, a comparison between the proposed and some existing antennas is addressed.

3.1. Reflection Coefficient

The fabricated prototype of the miniaturized dual-band CPW-fed antenna is displayed in Fig. 1(c). The designed antenna is printed on an FR4 substrate with a volume $20 \times 22 \times 0.8\,\text{mm}^3$. Fig. 6 depicts the measured and CST MWS and HFSS simulated reflection coefficient (S_{11}) results. Table 3 lists the performance parameters (impedance bandwidth (IBW), resonance frequency (f_r), and reflection coefficient $S_{11_{|f_r}}$) of the measured results and CST and HFSS simulated results. It is observed from Fig. 6 and Table 3 that the measured -10 dB IBW ($S_{11} \leq -10$ dB) of 3.16–3.75 GHz and 5.02–7.58 GHz with one resonance of 3.58 GHz in the 3.5 GHz WiMAX band and two resonances, 5.38 and 6.70 GHz, in the 6 GHz C band. The CST MWS (HFSS) simulated result reveals that the proposed antenna has resonance(s), IBW of 3.50 GHz, 3.22–3.80 GHz (3.50 GHz, 3.26–3.79 GHz), and 5.50 GHz, 6.80 GHz, 5.07–7.64 GHz (5.66 GHz, 6.94 GHz, 5.14–7.68 GHz). The simulated and measured results are in good agreement, and the discrepancy between them is due to the fabrication tolerance, losses coming from SMA soldering and substrate misalignment parameters, and calibration of VNA and connector wires.

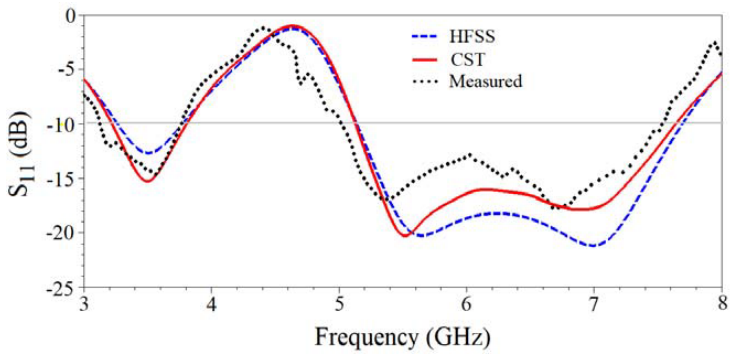

Figure 6. Comparison of CST and HFSS simulated reflection coefficient with measured results.

Table 3. Performance parameters (impedance bandwidth (IBW), resonance frequency (f_r) and reflection coefficient $S_{11_{|f_r}}$) of the measured results with CST MWS and HFSS simulated results.

Performance Parameters		CST MWS	HFSS	Measurement
−10 dB impedance Bandwidth (GHz)	Lower Band:	3.22–3.80	3.26–3.79	3.16–3.75
	Upper Band:	5.07–7.64	5.14–7.68	5.02–7.58
f_r (GHz)	Lower Band:	3.50	3.50	3.58
	Upper Band:	5.50, 6.80	5.66, 6.94	5.38, 6.70
$S_{11_{\|f_r}}$ (dB)	Lower Band:	−15.27	−12.83	−14.80
	Upper Band:	−20.22, −17.75	−20.21, −21.73	−16.80, −17.90

3.2. Surface Current Distribution

The surface current distributions of the designed antenna at three resonance frequencies 3.5, 5.5, and 7.5 GHz in addition to the notch frequency 4.55 GHz are portrayed in Fig. 7. As observed in Figs. 7(a)–(c), the currents at all three resonances are passed from the center strip of the CPW-fed line coupled to the outer boundary of the radiating patch with small amount of surface currents concentrated at

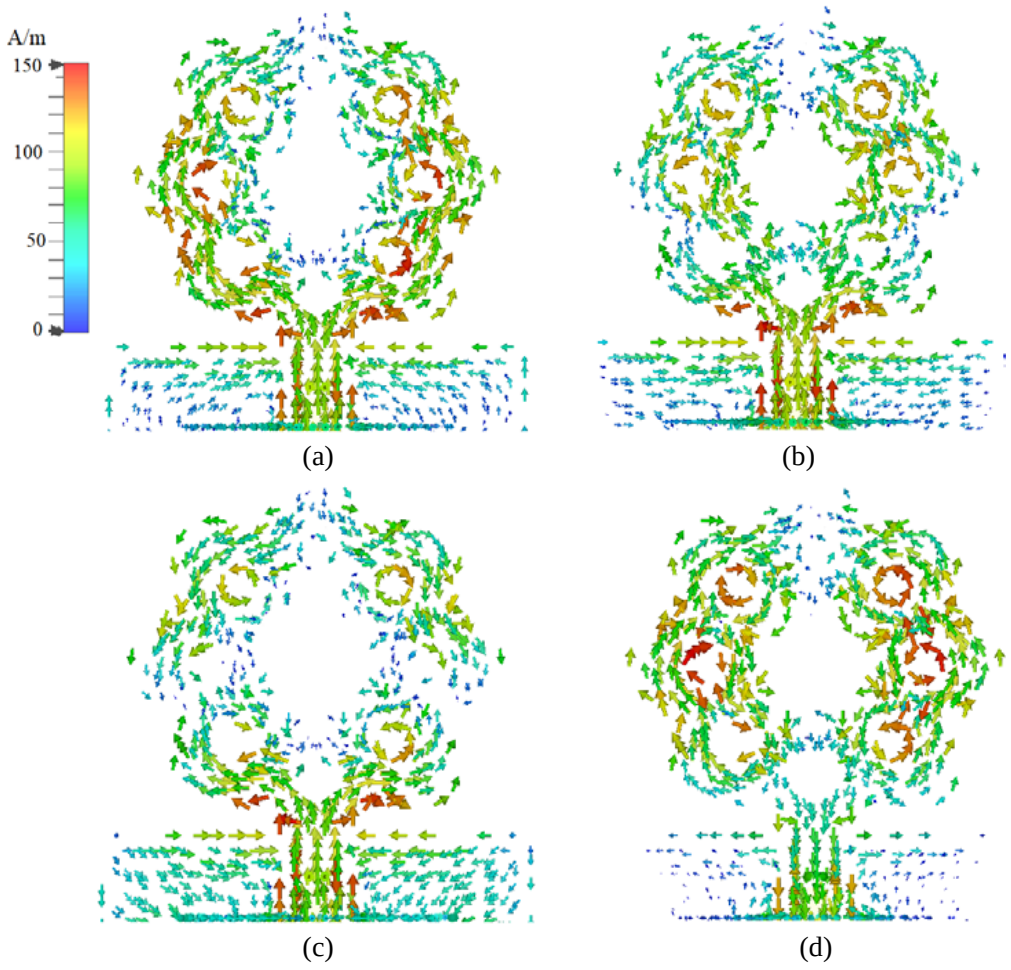

Figure 7. Current distribution of proposed antenna at three resonances (a) 3.5 GHz, (b) 5.5 GHz, and (c) 7.0 GHz and at notch frequency (d) 4.55 GHz.

patch's circular slots. However, at the notch frequency of 4.55 GHz as shown in Fig. 7(d), more current is distributed at the circular slit and at the boundary of the circular slots. Therefore, poor radiation occurs within the notched band resulting in decrease in antenna gain and efficiency. Good radiation and more gain and efficiency are exhibited by the proposed antenna in the two working passbands.

3.3. Far-Field Radiation Characteristic

The CST and HFSS simulated 2D radiation patterns of the designed antenna in H-plane (xoz-plane), right, and E-plane (xoy-plane), left, for 3.5, 5.5, and 7.0 GHz are shown in Fig. 8. As noticed in Fig. 8(a), for exciting by 3.5 GHz, the antenna had a nearly omnidirectional pattern in the H-plane and

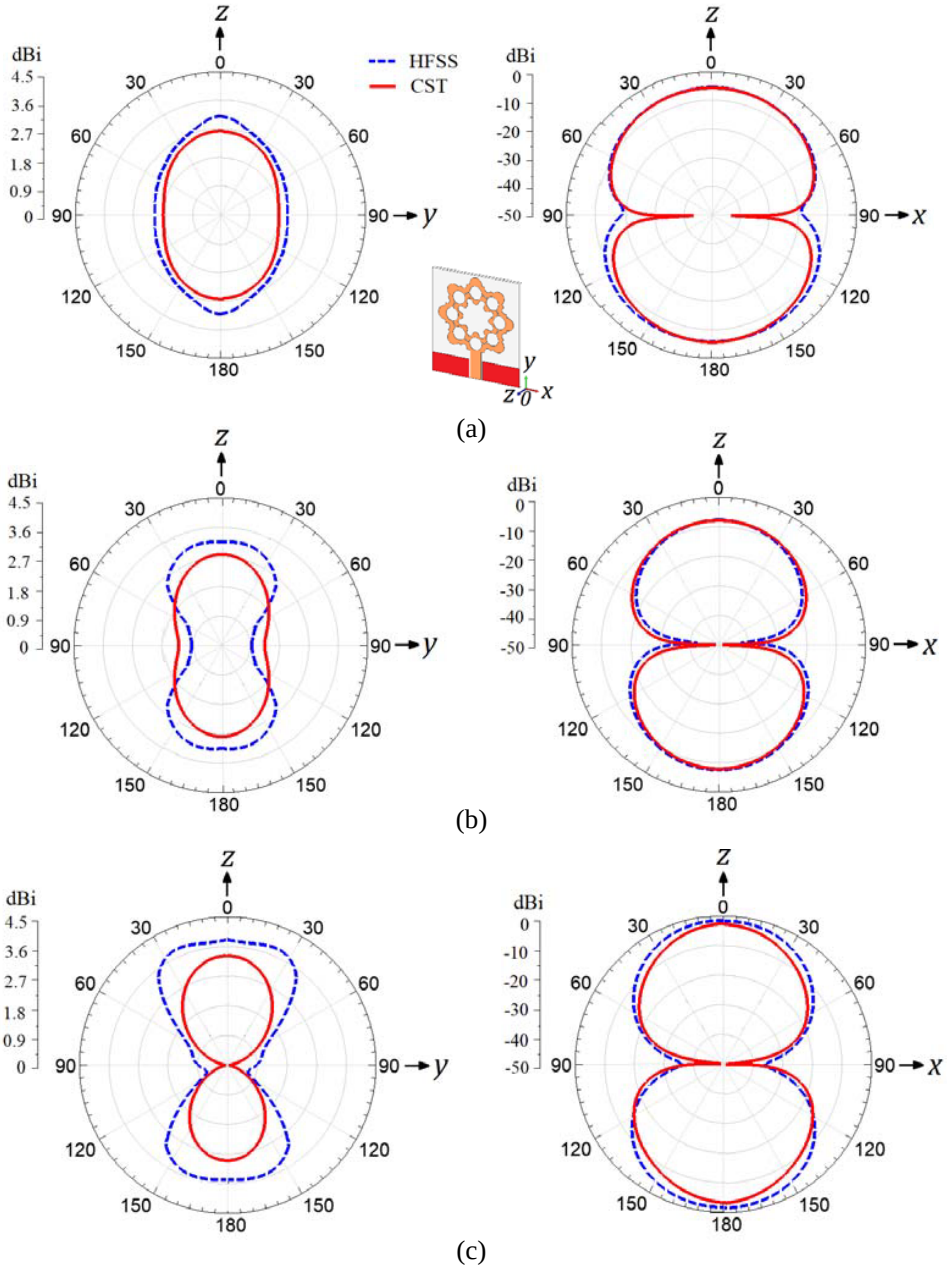

Figure 8. The CST and HFSS simulated 2D radiation pattern, E-plane or yoz-plane (left) and H-plane or xoz-pane (right), of the proposed antenna at three frequencies: (a) 3.5 GHz, (b) 5.5 GHz, and (c) 7.0 GHz.

a dipole-like pattern in the E-plane. At higher frequencies, 5.5 and 7.0 GHz, the radiation in H-plane is somewhat distorted to form a figure of eight, and in the E-plane the pattern is similar to that of the dipole antenna.

The 3D radiation patterns on the CST and HFSS simulator programs at the three resonance frequencies are depicted in Fig. 9. An omnidirectional radiation is achieved at 3.5 and 5.5 GHz, as noticed in Figs. 9(a) and (b), and a little distortion of radiation at y-axis direction occurs for higher frequencies (7 GHz), as portrayed in Fig. 9(c).

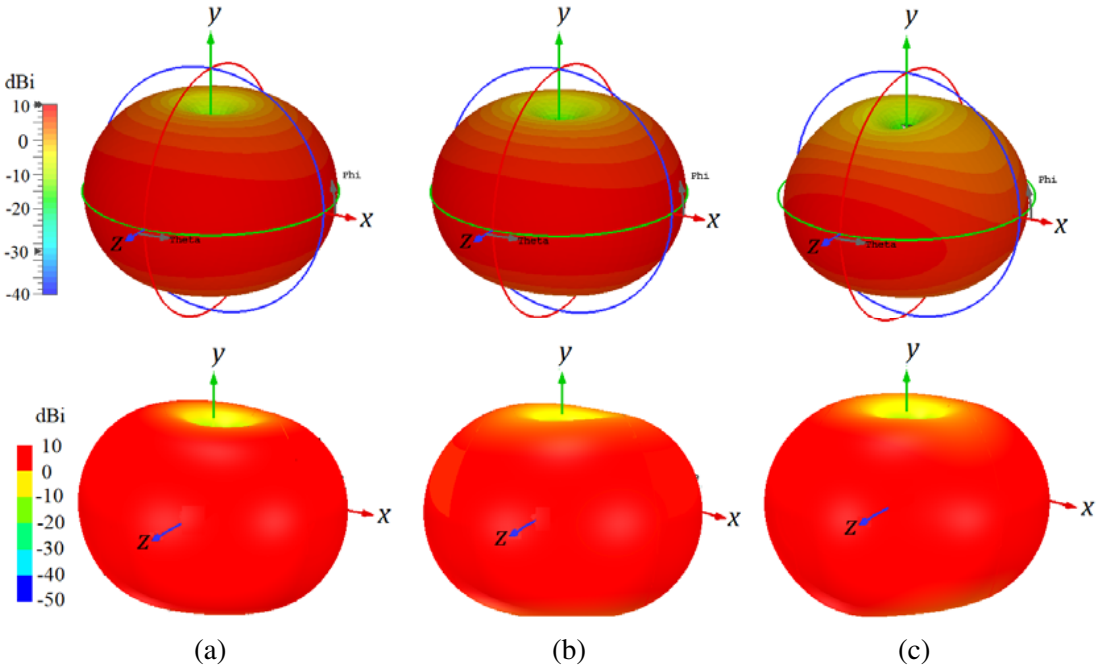

Figure 9. The CST (top) and HFSS (down) simulated 3D radiation patterns of the proposed antenna at three frequencies: (a) 3.5 GHz, (b) 5.5 GHz, and (c) 7.0 GHz.

3.4. Realized Gain and Efficiency

The simulated realized gain and efficiency against frequencies within the two working bands for the proposed antenna are plotted in Fig. 10, and Table 4 lists a comparison of peak gains and efficiencies obtained by CST MWS and HFSS. It is observed from Fig. 10(a) and Table 4 that the gain at the lower band has a peak gain of 2.05 dBi (CST) and 2.2 dBi (HFSS) whereas at the upper band the antenna peak gain is 3.62 dBi (CST) and 3.21 dBi (HFSS). As Fig. 10(b) and Table 4 show, the simulated CST (HFSS) peak antenna efficiencies at the lower and upper bands are 96% (94.2%) and 99.2% (96.10), respectively. These values of antenna gain and efficiency can be accepted for WiMAX and C-band applications.

Table 4. Comparison of simulated performance parameters (peak gain and efficiency) obtained by CST MWS and HFSS simulators.

Performance Parameters		CST MWS	HFSS
Peak gain (dBi)	Lower Band:	2.05	2.20
	Upper Band:	3.62	3.21
Peak efficiency (%)	Lower Band:	96.00	94.20
	Upper Band:	99.20	96.10

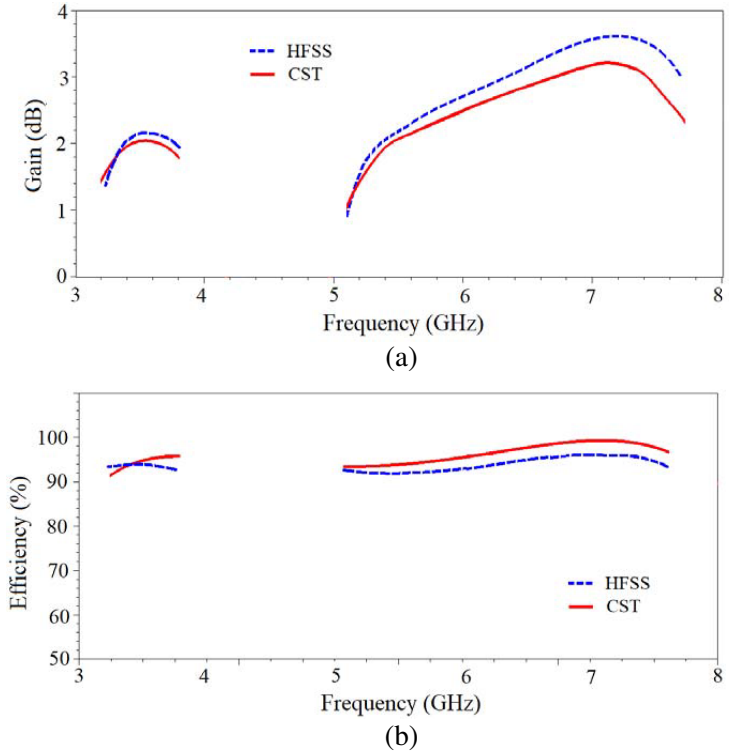

Figure 10. The CST and HFSS simulated (a) gain and (b) efficiency against frequency plot of proposed antenna.

Table 5. A comparison between recent reported dual-band antennas and the proposed antenna.

Ref.	Antenna size (mm^2)	Frequency bands	Feeding type	Antenna type	ε_r	h (mm)
[9]	22 × 22	(3.12–3.82) (5.15–5.83)	CPW	Pentagonal ring fractal antenna	4.4	1.6
[10]	30 × 45	(3.05–3.84) (5.24–7.54)	CPW	9-Point-star-shaped monopole	4.4	1.6
[11]	20 × 22	(3.06–3.89) (5.14–5.93)	CPW	two-arm strip with partial ground	4.4	1.6
[12]	20 × 22	(3.36–3.69) (4.35–6.00)	CPW	Meander folded-shaped monopole	4.4	1.6
[13]	24.5 × 20	(3.24–8.29) (9.12–11.2)	CPW	bow-tie-shaped patch and two asymmetric ground planes	4.4	1.6
[14]	17 × 18	(3.30–3.71) (5.70–5.94)	CPW	Semi-circular slotted antenna	4.4	0.8
[15]	17 × 20	(3.06–5.89)	CPW	Metamaterial-inspired hexagonal-shaped closed ring resonator	4.4	1.6
[16]	40 × 30	3.26–3.86 5.02–6.26	CPW	A wide circular slot and two pairs of symmetric planar inverted L strips	4.55	1.6
This work	20 × 22	3.15–3.75 5.02–7.58	CPW	Fractal slotted-ring monopole antenna (SRMA)	4.4	0.8

3.5. Comparison of Proposed Antenna with Other Existing Antennas

The comparison of proposed antenna with other recently reported antennas is summarized in Table 5. It is observed that the proposed antenna is characterized by a simple structure and compact size with two operating bands suitable for WiMAX and C-band applications. Only, Refs. [14] and [15] in Table 5 have smaller sizes than the designed antenna, but the antenna in [14] has narrow bands, especially the upper band, and in [15], the designed antenna covers only one operating wideband.

4. CONCLUSION

In this work, a new CPW-fed fractal slotted SRMA with dual-band operation for WiMAX and C-band applications has been presented. The proposed antenna is characterized by a simple structure and miniaturized size of $20 \times 22\,\text{mm}^2$. The notch frequency band is realized by inscribing a circular slit at the circular ring patch's center. By introducing circular fractal elements, antenna miniaturization with dual-band operation has been obtained. The optimally designed antenna with desired specifications was achieved after investigating in detail the parametric analysis of main geometric parameters, especially the circular slit's thickness. The surface current distributions at resonance frequencies and in particular at the notch frequency are studied to analyze the effect of circular slit for realizing the band notched feature. The prototype of the antenna was manufactured, and the measured results were compared with simulated ones, and reasonable agreement between them is achieved. The measured result of the fabricated antenna shows an impedance bandwidth at lower and upper bands of 600 MHz (3.15–3.75 GHz) and 2.56 GHz (5.02–7.58 GHz), respectively. It covers the WiMAX (3.3–3.8 GHz), sub-6 GHz bands, LTE 42/43 (3.4–3.8 GHz), LTE 46 (5.15–5.925 GHz), WLAN (5.1–5.825 GHz), and C band (4–8 GHz). Moreover, omnidirectional radiation with acceptable realized gain, and efficiency is exhibited by the proposed antenna.

REFERENCES

1. Mouhouche, F., K. Djafri, M. Dehmas, K. Chibane, and S. Ksentini, "A miniaturized quad band hexagon patch antenna for GSM1800, C band and WiMAX applications," *Frequenz*, Vol. 77, Nos. 3–4, 203–210, 2023, https://doi.org/10.1515/freq-2022-0046.
2. Vyas, K., G. Sanyal, A. K. Sharma, and P. K. Singhal, "Gain enhancement over a wideband in CPW-fed compact circular patch antenna," *International Journal of Microwave and Wireless Technologies*, Vol. 6, No. 5, 497–503, 2014, https://doi.org/10.1017/S1759078713001037.
3. Sang, S., B. Yuan, and T. Xiang, "Compact tri-band trapezoid CPW-fed antenna with SRR structure for WLAN/WiMAX applications," *Progress In Electromagnetics Research M*, Vol. 61, 177–184, 2017.
4. Ahmad, H., W. Zaman, S. Bashir, and M. Rahman, "Compact triband slotted printed monopole antenna for WLAN and WiMAX applications," *International Journal of RF and Microwave Computer-Aided Engineering*, Vol. 30, No. 1, e21986, 2020, https://doi.org/10.1002/mmce.21986.
5. Pandit, V. K. and A. R. Harish, "A compact CPW-fed tapered monopole triple-band antenna for WLAN/WiMAX application," *Microwave and Optical Technology Letters*, Vol. 60, No. 9, 2298–2303, 2018, https://doi.org/10.1002/mop.31340.
6. Hussain, N., A. Abbas, S.-M. Park, S. G. Park, and N. Kim, "A compact tri-band antenna based on inverted-L stubs for smart devices," *Computers, Materials and Continua*, Vol. 70, No. 2, 3321–3331, 2022, https://doi.org/10.32604/cmc.2022.020688.
7. Kunwar, A., A. K. Gautam, and B. K. Kanaujia, "Inverted L-slot triple band antenna with defected ground structure for WLAN and WiMAX applications," *International Journal of Microwave and Wireless Technologies*, Vol. 9, No. 1, 191–196, 2017, https://doi.org/10.1017/S1759078715001105.
8. Kumar, R., R. Sinha, A. Choubey, and S. K. Mahto, "A circular monopole antenna with uniquely packed quad T-shaped strips for WLAN/WiMAX application," *Frequenz*, Vol. 77, Nos. 3–4, 211–218, 2023, https://doi.org/10.1515/freq-2022-0017.

9. Naji, D. K., "Compact design of dual-band fractal ring antenna for WiMAX and WLAN applications," *International Journal of Electromagnetics and Applications*, Vol. 6, No. 2, 42–50, 2016, https://doi:10.5923/j.ijea.20160602.03.
10. Mandal, T. and S. Das, "Coplanar waveguide fed 9-point star shape monopole antennas for worldwide interoperability for microwave access and wireless local area network applications," *The Journal of Engineering*, Vol. 2014, No. 4, 155–160, 2014, https://doi.org/10.1049/joe.2013.0149.
11. Taghizadeh, H., C. Ghobadi, B. Azarm, and M. Majidzadeh, "Grounded coplanar waveguide-fed compact MIMO antenna for wireless portable applications," *Radioengineering*, Vol. 28, No. 3, 528–534, 2019, https://doi.org/10.13164/re.2019.0528.
12. Naji, D. K., "Design of compact dual-band and tri-band microstrip patch antennas," *International Journal of Electromagnetics and Applications*, Vol. 8, 26–34, 2018, https://doi.org/10.5923/j.ijea.20180801.02.
13. Alam, M. M., R. Azim, N. M. Sobahi, A. I. Khan, and M. T. Islam, "A dual-band CPW-fed miniature planar antenna for S-, C-, WiMAX, WLAN, UWB, and X-band applications," *Scientific Reports*, Vol. 12, No. 1, 7584, 2022, https://doi.org/10.1038/s41598-022-11679-7.
14. Naji, D. K., "Miniature slotted semi-circular dual-band antenna for WiMAX and WLAN applications," *Journal of Electromagnetic Engineering and Science*, Vol. 20, No. 2, 115–124, 2020, https://doi.org/10.26866/jees.2020.20.2.115.
15. Ameen, M., A. Mishra, and R. K. Chaudhary, "Asymmetric CPW-fed electrically small metamaterial-inspired wideband antenna for 3.3/3.5/5.5 GHz WiMAX and 5.2/5.8 GHz WLAN applications," *AEU — International Journal of Electronics and Communications*, Vol. 119, 153177, 2020, https://doi.org/10.1016/j.aeue.2020.153177.
16. Samsuzzaman, M., T. Islam, N. H. Abd Rahman, M. R. I. Faruque, and J. S. Mandeep, "Coplanar waveguide fed compact wide circular-slotted antenna for Wi-Fi/WiMAX applications," *International Journal of Antennas and Propagation*, 982958, 2014, https://doi.org/10.1155/2014/982958.
17. Balanis, C. A., *Antenna Theory: Analysis and Design*, John Wiley & Sons, Hoboken, NJ, 2016.